 MCB, vol.1, no.1, pp.37-52, 2004

Flaw tolerant bulk and surface nanostructures of biological systems

Huajian Gao[1], Baohua Ji[1], Markus J. Buehler[1], Haimin Yao[1]

Abstract: Bone-like biological materials have achieved superior mechanical properties through hierarchical composite structures of mineral and protein. Gecko and many insects have evolved hierarchical surface structures to achieve extraordinary adhesion capabilities. We show that the nanometer scale plays a key role in allowing these biological systems to achieve their superior properties. We suggest that the principle of flaw tolerance may have had an overarching influence on the evolution of the bulk nanostructure of bone-like materials and the surface nanostructure of gecko-like animal species. We demonstrate that the nanoscale sizes allow the mineral nanoparticles in bone to achieve optimum fracture strength and the spatula nanoprotrusions in Gecko to achieve optimum adhesion strength. In both systems, strength optimization is achieved by restricting the characteristic dimension of the basic structure components to nanometer scale so that crack-like flaws do not propagate to break the desired structural link. Continuum modeling and atomistic simulations have been conducted to verify the concept of flaw tolerance at nanoscale.

A simple tension-shear chain model has been developed to model the stiffness and fracture energy of biocomposites. It is found that, while the problem of low toughness of mineral crystals is alleviated by restricting the crystal size to nanoscale, the problem of low modulus of protein has been solved by adopting a large aspect ratio for the mineral platelets. The fracture energy of biocomposites is found to be proportional to the effective shear strain and the effective shear stress in protein along its path of deformation to fracture. The bioengineered mineral-protein composites are ideally suited for fracture energy dissipation as the winding paths of protein domain unfolding and slipping along protein-mineral interfaces lead to very large effective strain before fracture. The usual entropic elasticity of biopolymers may involve relatively small effective stress and may not be able to ensure simultaneous domain unfolding and interface slipping. Cross-linking mechanisms such as Ca^{++} induced sacrificial bonds in bone can increase the shear stress in protein and along the protein-mineral interface, effectively converting the behavior of entropic elasticity to one that resembles metal plasticity. The sacrificial bond mechanism not only builds up a large effective stress in protein but also allows protein deformation and interface slipping to occur simultaneously under similar stress levels, making it possible to engineer a very long range of deformation under significant stress in order to maximize energy absorption. Optimization of mineral platelets near theoretical strength is found to be crucial for allowing a large effective stress to be built up in protein via cross-linking mechanisms such as Ca^{++} induced sacrificial bonds. Similarly, for gecko adhesion, the strength optimization of individual spatulas is found to play a critical role in enhancing adhesion energy at the higher hierarchical level.

1 Introduction

An important objective of materials science and engineering has been to understand the relationships between microstructure of materials and their macroscopic properties. New challenges to this field in the 21^{st} century will include the development of multi-functional (e.g., strength, transport, self-repair, self-replicate, etc) and hierarchical (properties optimized at all length scales) materials systems. Nanotechnology promises to enable mankind to eventually design materials using a bottom-up approach, i.e. to construct multi-functional and hierarchical material systems by tailor-designing structures from atomic scale and up. However, currently we barely have any theoretical basis on how to design a hierarchical material system to achieve a particular set of functions. One strategy is to look among convergent evolutions in nature for hints on basic principles of multiscale and multifunctional materials design.

[1] Max Planck Institute for Metals Research, Heisenbergstrasse 3, D-70569, Stuttgart, Germany

It is only natural to seek inspirations from nature on solving technological problems. In fact, we have been doing so over the entire human history. Early inventers tried to develop ideas of flying by observing birds. Yet today we hardly think of mimicking birds in designing modern airplanes or space shuttles. Why is that so? How did we achieve today's advanced technology in aeronautical and aerospace engineering? A quick reflection will tell us that it is precisely the development of a thorough understanding of how birds fly by establishing theories of aerodynamics, solid mechanics and fluid mechanics that have allowed the birth of modern aeronautical, civil and many other industries. The route to success has been to uncover the basic principles and rules in nature to facilitate efficient engineering for human benefit. In this sense, biological systems perfected by natural evolution serve as models to study design principles for hierarchical and multi-functional material systems.

Biological materials, such as shell (Currey, 1977; Menig et al., 2000; Menig et al., 2001; Kamat et al., 2000; Jackson et al., 1988; Taylor, 1973; Currey and Taylor, 1974), tooth (Tesch et al., 2001; Weiner et al., 1999) and bone (Rho et al., 1998; Weiner and Wagner, 1998; Landis, 1995) exhibit many levels of hierarchical structures from macroscopic to microscopic length scales. The smallest building blocks in such materials are generally on the nanometer length scale. The enamel of tooth (Figs. 1a & e) is made of long, more or less needle-like crystals about 15-20 nm thick embedded in a soft matrix (Tesch et al., 2001; Warshawsky, 1989). The nanostructure of bone (Figs. 1b & f) consists of mineral crystal platelets with thickness around a few nanometers embedded in a collagen matrix (Landis, 1995; Landis and Hodgens, 1996; Roschger et al., 2001). Another familiar example is the "brick and mortar" structure of nacre (Figs. 1c & g) in which aragonite bricks with thickness around a few hundred nanometers are staggered and glued together by protein (Currey, 1977; Menig et al., 2000; Jackson et al., 1988). Apart from the hierarchical composite structures of these materials, a fundamental question is why the nanometer scale is so important. While the stiffness of biocomposites is similar to that of the mineral constituent, their fracture energy can be several orders of magnitude higher than that of the mineral. For example, nacre, as a composite of $CaCO_3$ and protein, has a fracture energy about 3000 times higher than that of the Monolithic $CaCO_3$ (Jackson et al., 1988). Generally, there is a well-defined organization of components in the biocomposite in the form of interlaced bricks separated by soft layers of protein gunk. Mineral platelets are separated and glued together by protein. The high toughness of biocomposites have been attributed to various mechanisms (Ji and Gao, 2004a) including their hierarchical structures (Menig et al., 2000; Menig et al., 2001; Kamat et al., 2000), the effects of mechanical properties of protein on dissipating fracture energy (Smith et al., 1999), protein-mineral interface roughness (Wang et al., 2001) and reduction of stress concentration at a crack (Okumura and Gennes, 2001).

Interesting nanostructures of biological systems for superior mechanical properties are not just limited to bone-like nanocomposites. Gecko and many insects have evolved elaborate hierarchical surface structures in their foot hair to achieve extraordinary adhesion capabilities. These animals possess ability to adhere to vertical surfaces and ceilings. A gecko is found to have hundreds of thousands of keratinous hairs or setae on its foot; each seta is $30\sim130$ μm long and contains hundreds of protruding nanoscale structures called spatula (Fig. 1d & h). Possible mechanisms of biological attachment include mechanical surface interlocking, fluid secretion (capillarity and viscosity) and molecular adhesion (van der Waals interaction). It is only until recently that the development of MEMS techniques have allowed the adhesive force of gecko to be accurately measured at the level of a single seta (Autumn et al., 2000), with evidence that the dominant adhesion mechanism of gecko is the van der Waals interaction (Autumn et al., 2002).

Why is nanoscale is so important to biological systems? What are the basic mechanisms and principles behind biological nanostructures? Motivated by these questions, we investigate mechanical properties of the bulk and surface nanostructures of bone-like and gecko-like biological systems, focusing on issues such as flaw tolerance, strength, stiffness and fracture energy.

2 The protein-mineral bulk nanostructure of bone-like biocomposites

2.1 Strength of mineral platelets

Experimental observations (Kamat et al., 2000; Wang et al., 2001; Fratzl et al., 1997; Tesch et al., 2001; Landis, 1995; Landis and Hodgens, 1996) have shown that, at the most elementary structure level, biological mate-

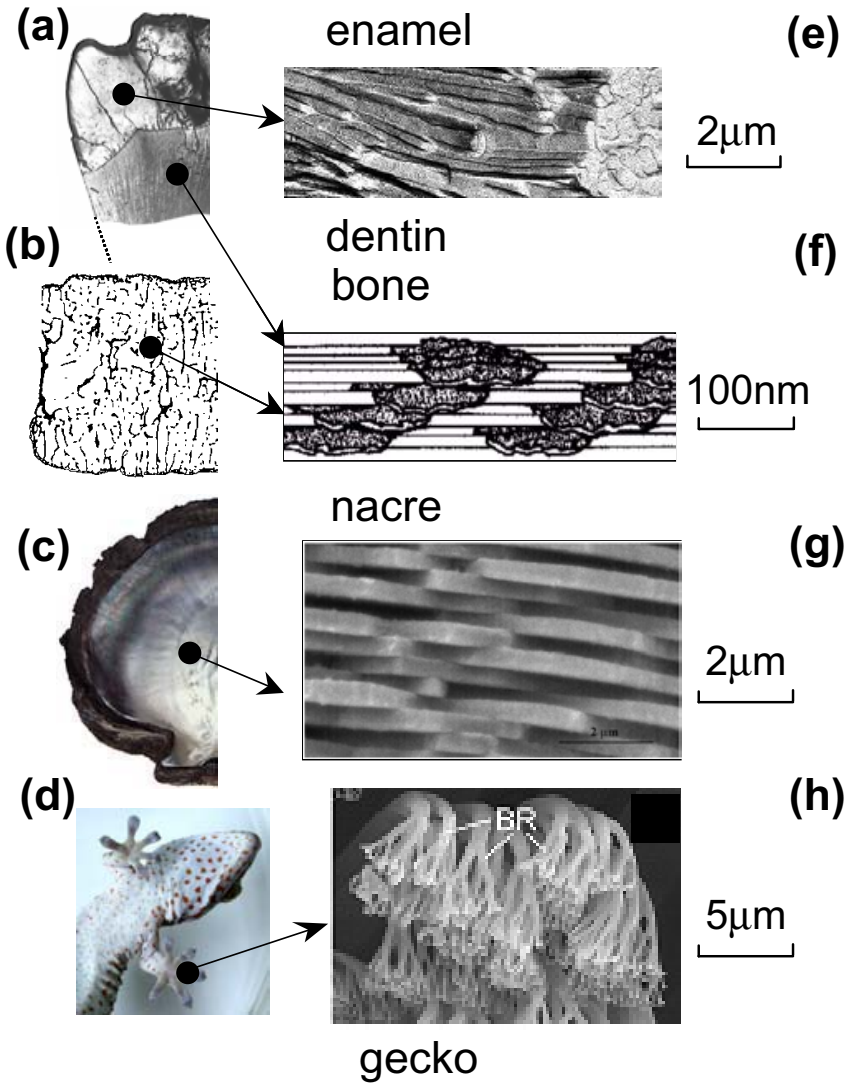

Figure 1 : Bulk and surface biological nanostructures. Many hard biological tissues, such as tooth (a), vertebral bone (b) and shells (c) are made of nanocomposites with hard mineral platelets in a soft (protein) matrix. Enamel (e) is made of long, more or less needle-like crystals about 15-20 nm thick and 1000 nm long, with a relatively small volume fraction of a soft protein matrix. Dentin and bone (f) are made of plate-like crystals (2-4 nm thick, up to 100 nm long) embedded in a (collagen-rich) protein matrix. The volume ratio of mineral to matrix is on the order of 1:2. Nacre (g) is made of plate-like crystals (200-500 nm thick and a few micrometers long) with a very small amount of soft matrix in-between. All the composites share the structural feature of hard platelets with a very large aspect ratio, arranged parallel in a brick-and-mortar-like fashion. The adhesive system of Gekko gecko has evolved surface nanostructure for adhesion. A toe of gecko (d) contains a terminal nanostructure called spatula about 200-500 nm in diameter (h).

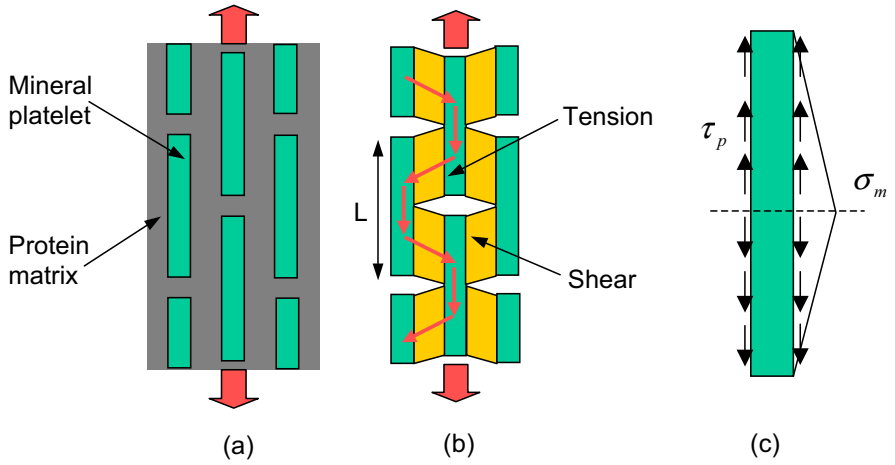

Figure 2 : A simple tension-shear chain model of biocomposites. (a) A schematic diagram of staggered mineral crystals embedded in a soft (protein) matrix. (b) The tension-shear chain model showing the path of load transfer in the mineral-protein composites. The mineral platelets carry tensile load and the protein transfers loads between the platelets via shear. (c) The free body diagram of a mineral platelet showing the shear stress applied on the surface of the platelet by protein.

rials exhibit a generic structure consisting of staggered mineral platelets embedded in a soft matrix, as shown in Fig. 2(a). Jaeger and Fratzl (2000) discussed different arrangements of mineral platelets in collagen fibril and provided simple estimates for the stiffness of biocomposites. Under an applied tensile stress, the path of load transfer in the mineral-protein biocomposites can be represented by a tension-shear chain model (Gao et al., 2003) depicted in Fig. 2 where the mineral platelets carry tensile load and the protein transfers load between mineral crystals via shear. In this tension-shear chain model, the mineral-protein composite is simplified to a one-dimensional chain consisting of tensile springs (mineral) interlinked by shear springs (protein).

The integrity of the composite chain structure shown in Fig. 2(b) is hinged upon the strength of mineral platelets since breaking of the platelets would destroy the critical structural links in the composite, leading to disintegration of the protein-mineral network. It will be discussed shortly (section 2.3) that the strength of mineral platelets plays a crucial role in the fracture energy of the composite. In order to achieve high fracture energy, the mineral platelets must be able to sustain large tensile stress without fracture; the protein and the protein-mineral interface must be able to absorb and dissipate a large amount of energy by undergoing large deformation under large stress. How to optimize the strength of the mineral platelets? The Griffith theory of fracture (Griffith, 1921) and common engineering experiences have shown that the strength of brittle solids is determined by pre-existing flaws. Gao et al. (2003) pointed out that the nanometer scale is the key to optimizing mineral strength. At the simplest level, this can be understood from the following consideration. A perfect, defect-free mineral particle should be able to sustain mechanical stress near the theoretical strength σ_{th} of the material. However, we assume that the particle contains crack-like flaws. For example, protein molecules trapped within the mineral crystals during the biomineralization process are mechanically equivalent to embedded microcracks and may precipitate brittle fracture. Consider a thumbnail crack in the mineral particle as shown in Fig. 3(a). The strength of this "cracked" mineral platelet can be calculated from the Griffith criterion of fracture as

$$\sigma_m^f = \alpha E_m \Psi, \quad \Psi = \sqrt{\frac{\gamma}{E_m h}}, \tag{1}$$

where γ is the surface energy and h is the thickness of mineral crystal. The parameter α depends on the crack geometry and is approximately equal to $\sqrt{\pi}$ for a half-cracked platelet (i.e. maximum crack depth equals one half of the platelet thickness). Figure 3(c) compares the strength of the cracked crystal with that of a defect-free crystal. We see that there exists a transition between

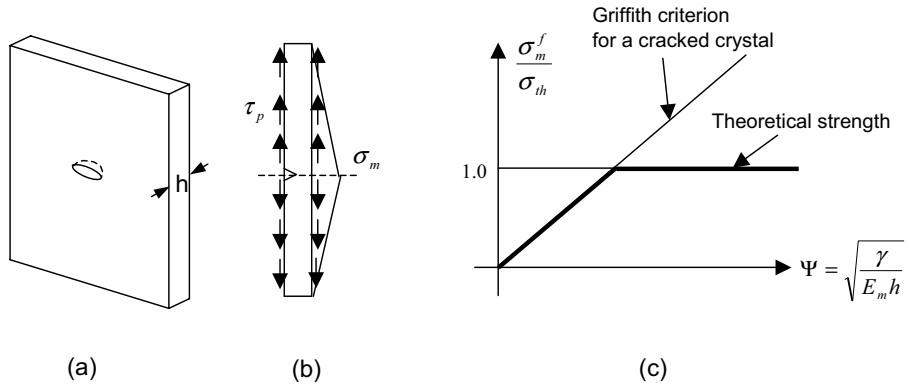

Figure 3 : A length scale for optimized strength in mineral platelet. (a) A schematic diagram of mineral platelet with a surface crack. (b) The load distribution on the cracked mineral crystal. (c) Comparison of the strength of a cracked mineral platelet calculated from the Griffith criterion with the strength of a perfect, defect-free crystal.

crack propagation governed by the Griffith criterion and uniform rupture of atomic bonds at theoretical strength at a critical length scale (Gao et al., 2003)

$$h_{cr} \approx \alpha^2 \frac{\gamma E_m}{\sigma_{th}^2}. \quad (2)$$

At this length scale, the fracture mechanism changes from energy governed flaw propagation to strength governed structure disintegration. Below the critical length of eq. (2), the fracture strength of a cracked crystal is near that of a perfect crystal because the Griffith criterion for crack propagation can not be satisfied before the applied stress reaches a level near the theoretical strength of material. Taking a rough estimate γ=1 J/m^2, E_m= 100 GPa, and $\sigma_{th} = E_m/30$, we find h_{cr} to be around 30 nm for a half-cracked platelet. The nanometer scale not only allows the strength of mineral particles to be optimized near theoretical strength but also renders these particles insensitive to crack-like defects (flaw tolerance). For larger mineral particles above the critical length, we have the conventional engineering concepts that the strength is determined by pre-existing flaws and the failure occurs by propagation of flaws under stress concentration. As the mineral size drops below the critical length, the strength of a perfect mineral platelet is maintained despite of defects. The failure criterion is governed by theoretical strength rather than by the Griffith criterion, and the material becomes insensitive to flaws. Based on this analysis, Gao et al. (2003) made a hypothesis that the nanometer size of mineral crystals in biocomposites is selected to ensure optimum fracture strength and flaw tolerance (for robustness).

The bio-inspired length scale for optimum mineral strength

$$\gamma E_m / \sigma_{th}^2 \quad (3)$$

is an intrinsic material parameter which measures the size of fracture process zone in a brittle material. Depending on the geometry of structure and crack, this can range from a few nanometers to a few tens of nanometers. As the structural size reaches this critical length, materials become insensitive to flaws in the sense that pre-existing cracks no longer propagate in the structure.

2.2 Stiffness of biocomposites

We have discussed how the nanometer scale allows the mineral bits in biological materials to achieve optimum strength and flaw tolerance. The problem of low toughness of mineral crystals is thus alleviated by restricting the crystal size to nanoscale. How does nature solve the problem of low modulus of protein? We now proceed to discuss the stiffness and fracture energy of biocomposites based on the tension-shear chain model depicted in Fig. 2(b). We immediately note that the simple chain model may be overly simplistic in many aspects, including neglect of the three dimensional character of deformation fields in biocomposites. However, here we adopt the view that simple models can still be very useful as long as their limitations are well understood. Gao et al. (2003) and Ji and Gao (2004b) have used the chain model of Fig. 2(b) to estimate the composite stiffness and found

results in reasonable agreement with a full finite element analysis of biocomposites. In this paper, we further generalize this model to account for nonlinear behavior of protein deformation and to estimate the fracture energy of biocomposites.

Applying force equilibrium to a single mineral platelet (Fig. 2c) indicates that the tensile stress in a mineral platelet varies linearly with the distance x from the center of the platelet,

$$\tilde{\sigma}_m(x) = \sigma_m \frac{L-2|x|}{L}. \tag{4}$$

The maximum stress occurs near the center of the platelet and is related to the shear stress of protein as,

$$\sigma_m = \rho\tau_p \tag{5}$$

where ρ is the aspect ratio of the mineral platelets. The average stress in the composite is

$$\sigma = \frac{1}{2}\Phi\sigma_m = \frac{1}{2}\rho\Phi\tau_p \tag{6}$$

where Φ denotes the volume concentration of mineral. The average strain in the composite structure obeys the kinematical relationship

$$\varepsilon = \frac{\Delta_m + 2\varepsilon_p h(1-\Phi)/\Phi}{L} \tag{7}$$

where Δ_m is the elongation of the mineral platelets, ε_p is the shear strain of protein and L is the length of mineral shown in Fig. 2(b). We note that eqs. (4-7) remain valid even for nonlinear behaviors as long as the shear strain in protein can still be regarded as approximately uniform.

The composite stiffness (Young's modulus) E can be obtained by considering infinitesimal deformations in the composite, in which case

$$\Delta_m = \frac{\sigma_m L}{2E_m}, \quad \varepsilon_p = \frac{\tau_p}{G_p} \tag{8}$$

where E_m is the Young's modulus of mineral and G_p is the shear modulus of protein. Inserting eq. (8) into eq. (7) while making use of eq. (6) yields an estimate for the composite stiffness (Gao et al., 2003),

$$\frac{1}{E} = \frac{4(1-\Phi)}{G_p \Phi^2 \rho^2} + \frac{1}{\Phi E_m}. \tag{9}$$

Ji and Gao (2004b) have verified that eq. (9) agrees well with finite element calculations. Normally, G_p is much smaller (up to 3 orders of magnitude) than E_m. For small aspect ratios, the second term can be neglected so that the composite stiffness behaves as $E \propto G_p\rho^2$, indicating that the composite stiffness can be rapidly amplified with respect to that of protein via aspect ratio. The simple expression in eq. (9) indicates that the large aspect ratio of mineral particles compensates for the low modulus of the protein phase since it is the combination $\rho^2 G_p$ which appears in the expression for the composite stiffness. In other words, biocomposites are stiffened relative to protein by the square of the aspect ratio of mineral crystals. An aspect ratio of 30-40 would provide a magnification of 3 orders of magnitude over the stiffness of protein and bring the composite stiffness close to that of mineral.

2.3 Fracture energy of biocomposites

We now consider the fracture energy of biocomposites. Consider a crack as shown in Fig. 4. For simplicity, we assume that dissipation of fracture energy near the crack tip is concentrated within a strip of localized deformation along the prospective crack path (Fig. 4), reminiscent of the classical Dugdale model (Dugdale, 1960) of plastic yielding near a crack in a ductile sheet. In such a cohesive strip model, the fracture energy can be calculated from the integral (Klein and Gao, 1998; Gao and Ji, 2003)

$$J_c = w\int \sigma(\varepsilon)d\varepsilon \tag{10}$$

where w is the width of the localization strip and $\sigma = \sigma(\varepsilon)$ is the continuum cohesive law of the biocomposite. To evaluate the integral in eq. (10), we generalize the simple tension-shear chain model of Fig. 2(b) to accounting for large deformation of protein within the fracture process zone.

We assume mineral particles are strong enough to retain their integrity during composite fracture. In this case, the width of the fracture localization zone w should be larger than, and proportional to, the length L of mineral particles. Therefore, we write

$$w = \xi L, \quad \xi \geq 1. \tag{11}$$

Inserting eqs. (6) and (7) into the integral of eq. (10) leads to

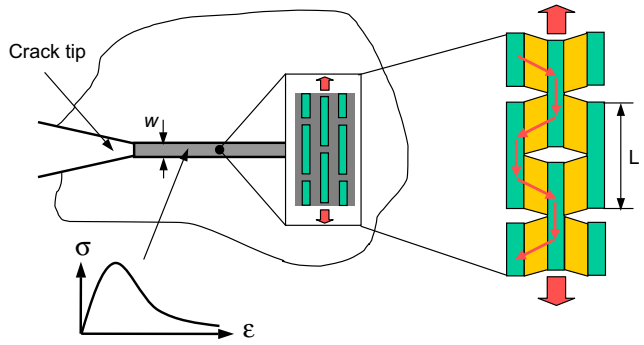

Figure 4 : A Dugdale-type estimate for the fracture energy of biocomposites. The fracture energy dissipation is assumed to concentrate within a strip of localized deformation with width w. The tension-shear chain model is used to estimate the fracture energy in the localization strip. The stress and strain relation of material within the localization strip is assumed to obey a cohesive law.

$$J_c = \xi L \int \sigma d\varepsilon = \frac{1}{2}\Phi\xi \int \sigma_m d\Delta_m + \xi(1-\Phi)L \int \tau_p d\varepsilon_p. \tag{12}$$

In eq. (12), the first term corresponds to the contribution of mineral and the second term that of protein to the fracture energy of biocomposite. The contribution from the deformation of brittle mineral particles to the composite fracture energy is generally expected to be negligibly small in comparison with that from protein deformation. We neglect the first term in eq. (12) and write

$$J_c = \xi(1-\Phi)L \int \tau_p d\varepsilon_p = \xi(1-\Phi)L\tau_p^* \varepsilon_p^f \tag{13}$$

where ε_p^f is the effective shear strain of protein before fracture and τ_p^* is the effective shear stress in protein. The effective strain of protein should include both the deformation of protein molecules as their domains unfold and slipping along the protein-mineral interface. The effective shear stress in protein can be expressed as

$$\tau_p^* = \min(\tau_p^f,\ \tau_{int}^f,\ \sigma_m^f/\rho) \tag{14}$$

where τ_p^f measures the stress associated with domain unfolding, τ_{int}^f is the strength of interface and σ_m^f is the tensile strength of mineral.

Therefore, a simple estimate of the fracture energy of biocomposites is given by

$$J_c = \xi(1-\Phi)L\varepsilon_p^f \min(\tau_p^f,\ \tau_{int}^f,\ \sigma_m^f/\rho). \tag{15}$$

This simple estimate suggests that the toughness of biocomposites increases with (i) the volume fraction of protein $(1-\Phi)$, (ii) the length of mineral particle L, (iii) the effective strain of protein ε_p^f before fracture, and (iv) the effective stress of protein which is bounded by the stress τ_p^f required for protein domain unfolding, the protein-mineral interface strength τ_{int}^f, and the mineral strength σ_m^f. Among these parameters, the effect of volume fraction of protein is clear: The more protein, the more volume of materials for energy dissipation. Baring mineral fracture, the mineral particle length sets an intrinsic length scale for strain localization near the crack tip: The longer the mineral, the more delocalized the crack-tip deformation and the larger the fracture energy. The effective shear strain of protein before fracture is a key parameter for fracture energy. Protein molecules can undergo large deformation as the protein domains unfold (Smith et al., 1999), and are thus naturally engineered with long ranges of deformation before fracture. Slipping along the protein-mineral interface further increases the effective strain. The effective shear stress of protein is determined by the lower bound of protein strength, interfacial strength and mineral strength. A key to increase the first two has been attributed to Ca^{++} induced sacrificial bonds in bone (Thompson et al., 2001). In other words, the protein stress is limited by the weakest of three different deformation mechanisms, protein unfolding, interface slipping, and mineral fracture. Under the optimum condition, the strengths governing each of the three mechanisms would be identical to each other, i.e.

$$\tau_p^f = \tau_{int}^f = \sigma_m^f/\rho. \tag{16}$$

This immediately suggests an optimum mineral aspect ratio $\rho^* = \sigma_m^f \big/ \tau_p^f$. Assuming that the mineral strength obeys the Griffith criterion $\sigma_m^f = \sqrt{\alpha^2 \gamma E_m / h}$, Gao et al. (2003) obtained the following estimate for the optimum aspect ratio

$$\rho^* = \frac{\sigma_m^f}{\tau_p^f} = \frac{1}{\tau_p^f}\sqrt{\frac{\alpha^2 \gamma E_m}{h}}. \tag{17}$$

This equation shows that the optimum aspect ratio of mineral platelets is inversely proportional to the square

root of the mineral thickness: the smaller the platelets, the larger the optimal aspect ratio. The mineral crystals in bone have thickness on the order of a few nanometers and aspect ratio 30–40 and those in nacre have thickness on the order of a few hundred nanometers and aspect ratio around 10, which roughly corresponds to the scaling law predicted by eq. (17).

Equation (16) also shows why it is necessary to have strong mineral crystals to achieve high fracture energy. Since large aspect ratio $\rho = 30 \sim 40$ is needed to compensate for the low modulus of protein, the mineral strength must exceed

$$\sigma_m^f \geq (30 \sim 40)\tau_{int}^f. \tag{18}$$

In biological materials, the organic molecules and the inorganic mineral crystals are locally polarized and the interface strength is dominated by electrostatic interactions. Taking τ_{int}^f to be around (20-50) MPa, we can immediately estimate from eq. (18) that the mineral strength σ_m^f needs to be on the order of a few GPa, which is near the theoretical strength of mineral. The analysis explained, from a different perspective, why it is important to have the size of mineral platelets chosen at the nanoscale: High strength, flaw tolerant mineral crystals are crucial to maintain a significant effective stress in protein which, together with large shear deformation inside protein and along the protein-mineral interface, gives high fracture energy, as shown by eq. (15).

The hierarchical structures of proteins are ideally suited for absorbing and dissipating fracture energy. Proteins in nacre deform by gradual unfolding of their domain structures (Smith et al., 1999). It can take a large amount of deformation before the primary structure of protein, the peptide backbone, is directly stretched. Thus the molecular design of proteins is ideally suited for absorbing fracture energy. However, large deformation alone is not sufficient as it is the area under the stress-strain curve which defines the fracture energy. According to eq. (15), a large effective stress in protein is also needed for the high toughness of biocomposites. The usual entropic elasticity of biopolymers involves relatively small effective stress. A solution to this problem in bone has been provided by the mechanism of sacrificial bonds in which Ca^{++} ions cross-link peptides with negative electric charges, forming relatively strong bonds with strength up to 30% of the covalent bonds of the peptide backbone (Thompson et al., 2001). The sacrificial bonds bind functional groups along different segments of protein and along the protein-mineral interface, increasing the effective stress in protein and leading to high fracture energy. The sacrificial bonds not only build up a large effective stress in protein but also allow protein deformation and interface slipping to be able to occur simultaneously under similar stress levels, making it possible to engineer a maximum range of shear deformation. Figure 5 schematically shows the mechanism of sacrificial bonds in bone where protein molecules between mineral platelets deform as sacrificial bonds formed by Ca^{++} ions break sequentially, resulting in a very long flat tail of the force-extension $(F-u)$ curve with saw tooth undulation (Thompson et al., 2001). In general, cross-link mechanisms such as Ca^{++} induced sacrificial bonds effectively can play an important role in converting entropic elasticity behavior to one that resembles metal plasticity, hence enhancing the capability of polymers to absorb fracture energy. This seems to be an important principle in design of energy absorbing organic-inorganic composite materials.

3 Flaw tolerant surface nanostructure of gecko for adhesion

3.1 Saturation of adhesion strength of spatula at nanoscale

The concept of nanoscale flaw tolerance can be discussed in a more general context to include the surface nanostructure of gecko. Among the hairy biological attachment systems, the density of surface hairs (setae) increases with the body weight of animal, and gecko has the highest density among all animal species that have been studied (Scherge and Gorb, 2001). Various mechanical models have been developed to model specific hairy attachment systems, for instance the fiber arrays structure (Persson, 2003; Hui et al., 2002). In particular, the Johnson-Kendall-Roberts (JKR) model (Johnson et al., 1971) of contact mechanics has been used to show that splitting of a single contact into multiple smaller contacts always results in enhanced adhesion strength (Arzt et al., 2002, 2003; Autumn et al., 2002).

The most terminal (smallest) structure of gecko's attachment mechanism is called spatula (Fig. 1h) which is about 200-500 nanometers in diameter. Why is the spatula size in the nanometer range? To understand this, we have modeled the spatula as an elastic flat-ended cylin-

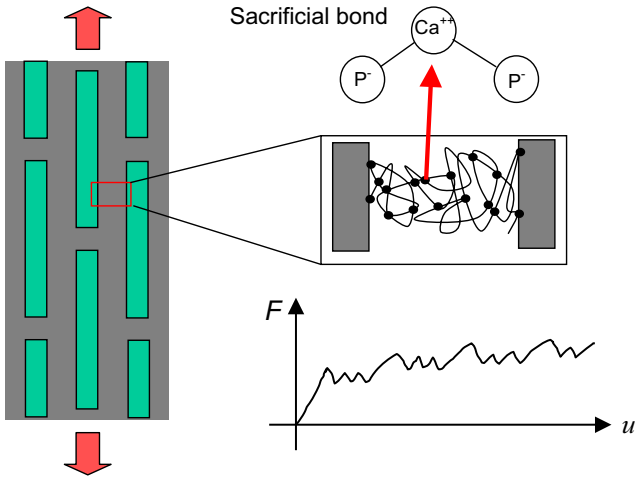

Figure 5 : A schematic illustration of protein modules deforming between mineral platelets in the biological nanostructure and the inherent force-extension relation of protein with cross-linking mechanism of Ca^{++} formed sacrificial bonds. The sacrificial bonds are formed by Ca^{++} ions linking negatively charged functional groups along the peptide chain. The sacrificial bonds effectively convert the usual entropic elasticity behaviors of biopolymers to one that resembles metal plasticity. The long flat tail and the saw tooth undulation of protein deformation (Smith et al, 1999; Thompson et al., 2001) are due to breaking of sacrificial bonds and protein unfolding in the modules instead of molecular backbone.

drical hair in adhesive contact with a rigid substrate (Gao et al., 2004). The radius of the cylinder is R. To test the ability of the flat cylinder to adhere in the presence of adhesive flaws, imperfect contact between the spatula and substrate is assumed such that the radius of the actual contact area is $a = \alpha R$, $0<\alpha<1$, as shown in Fig. 6(b); the outer rim $\alpha R < r < R$ represents flaws or regions of poor adhesion. The adhesive strength of such an adhesive joint can be calculated by treating the contact problem as a circumferentially cracked cylinder, in which case the stress field near the edge of the contact area has a square-root singularity with stress intensity factor (Tada et al., 2000)

$$K_I = \frac{P}{\pi a^2}\sqrt{\pi a}F_1(\alpha) \tag{19}$$

where $F_1(\alpha)$ varies in a narrow range between 0.4 and 0.5 for $0 \le \alpha \le 0.8$ ($\alpha = 1$ corresponds to perfect, defect-free contact). Substitute eq. (19) into the Griffith condition

$$\frac{K_I^2}{2E^*} = \Delta\gamma \tag{20}$$

where the factor 2 is due to the rigid substrate. The apparent adhesive strength normalized by the theoretical strength for adhesion, $\hat{\sigma}_c = P_c/(\sigma_{th}\pi R^2)$, is obtained as

$$\hat{\sigma}_c = \beta\alpha^2\psi \tag{21}$$

where

$$\psi = \sqrt{\frac{\Delta\gamma E^*}{R\sigma_{th}^2}}, \tag{22}$$

$$\beta = \sqrt{2/\left(\pi\alpha F_1^2(\alpha)\right)}, \quad E^* = E/(1-\nu^2) \tag{23}$$

E and ν being the Young's modulus and Poisson's ratio, respectively. The adhesive strength is a linear function of the dimensionless variable ψ with slope $\beta\alpha^2$. The maximum adhesion strength is achieved when the pull-off force reaches $P_c = \sigma_{th}\pi a^2$, or $\hat{\sigma}_c = \alpha^2$, in which case the traction within the contact area uniformly reaches the theoretical strength σ_{th}. This saturation in strength occurs at a critical size of the contact area

$$R_{cr} = \beta^2\frac{\Delta\gamma E^*}{\sigma_{th}^2}. \tag{24}$$

Figure 6(c) plots the apparent adhesive strength for α=0.7, 0.8 and 0.9, together with the case of flawless contact (α=1). The corresponding result of a hemispherical tip based on the JKR model is plotted as a dashed line for comparison. (In plotting the JKR curve, we have taken E^*/σ_{th} to be 75). The flat-ended spatula achieves the maximum adhesion strength much more quickly than the hemispherical configuration.

The critical contact size for saturation of adhesion strength can be estimated as follows. Assume the actual contact area is about 50% of the total area available for contact, corresponding to $\alpha \cong 0.7$. The parameters for the van der Waals interaction and the Young's modulus of spatula (keratin) are selected as follows:

$$\sigma_{th} = 20MPa, \quad \Delta\gamma = 0.01J/m^2, \quad \frac{\Delta\gamma}{\sigma_{th}} \cong 0.5nm,$$
$$E^* = 2GPa. \tag{25}$$

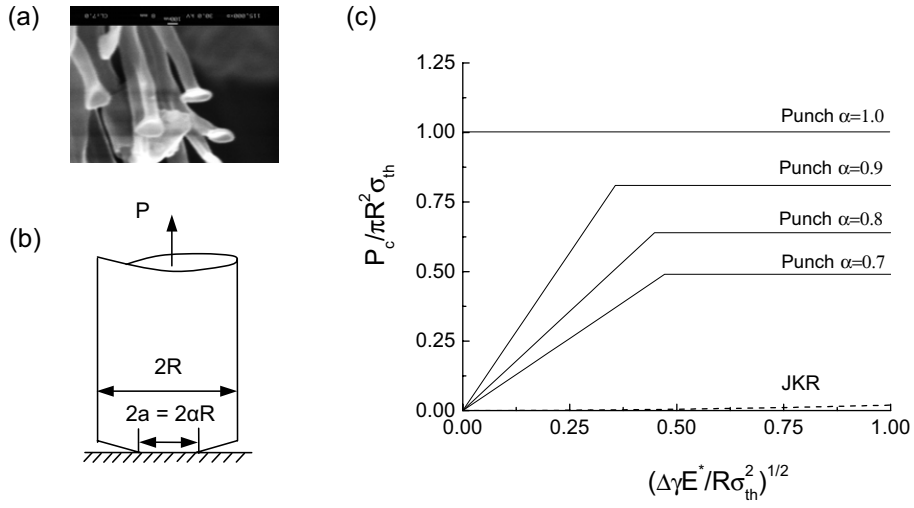

Figure 6 : Adhesion of a flat-ended cylinder to a rigid substrate. The actual contact area is assumed to be smaller than the total area of the punch due to imperfections along the outer rim of the punch. This contact model is elastically equivalent to a cracked cylinder. (a) A bundle of spatulas. (b) The geometry of a flat punch partially adhering to a substrate. (c) Variations of the apparent adhesion strength for different actual contact areas according to Griffith criterion and theoretical strength. The JKR prediction of a hemispherical tip is plotted as a dashed line for comparison. The plot shows that a flat punch induces much larger adhesive forces in comparison with a hemispherical tip, and that the adhesion strength reaches the theoretical strength of van der Waals interaction at a critical contact size.

This gives the critical size for adhesive strength saturation as

$$R_{cr} \cong 225\,\text{nm}. \tag{26}$$

Interestingly, the radius of gecko's spatula is typically around 100-250 nm. The above analysis suggests that the nanometer size of the spatula structure of gecko may have been evolved to achieve optimization of adhesive strength in tolerance of possible contact flaws.

3.2 Adhesion energy of spatula arrays

To relate the adhesion strength of a single spatula to the adhesion energy of an array of spatulas, consider an array of hairs in adhesive contact with a substrate, as shown in Fig. 7. The Young's modulus and adhesive strength of a single spatula are E and σ_c. The adhesion energy of the spatula array analogous to eq. (15) is

$$J_c = L\int \sigma d\varepsilon = \frac{L\sigma_c^2\varphi}{2E} \tag{27}$$

where L is the length of spatula and φ is the areal density of contact regions. Thus the adhesion energy of spatula structure is proportional to the square of the adhesive strength of single spatulas. It is therefore desirable to reduce the size of spatula to near the critical size so as to maximize the adhesive strength and to increase the adhesion energy of an array. It is also helpful to increase the contact area density φ and the length L of spatula. However, these parameters may be affected by roughness of substrate as well as the condition that the spatula array must be stable against self-bunching (Hui et al., 2002; Gao et al., 2004).

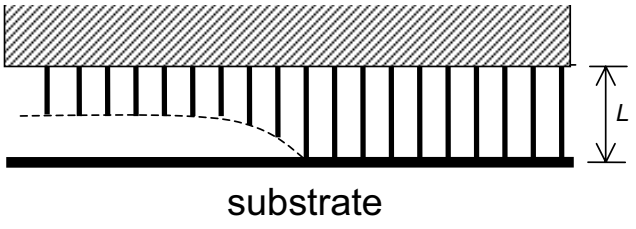

Figure 7 : An illustration of detachment of an array of hairs in adhesive contact with a substrate. The adhesion energy of the array can be estimated by calculating energy absorbed in the layer as individual hairs detach from the substrate.

The mechanism of fracture energy dissipation in protein-mineral biocomposites is very different from that in the spatula array. In the case of protein-mineral composites, fracture energy is predominantly dissipated through shear deformation in protein and slipping along the protein-mineral interface. Optimization of mineral platelets near theoretical strength is crucial for allowing a large effective stress to be built up in protein via cross-link mechanisms such as Ca^{++} induced sacrificial bonds in bone. In the case of the spatula structure, the adhesive strength of individual spatulas directly affects the adhesion energy of the array. It is interesting to observe that, in both systems, strength optimization is achieved by restricting the characteristic dimension of the basic structure components to nanometer scale so that crack-like flaws do not propagate to break the desired structural link.

4 Atomistic simulations of the flaw tolerance concept

The concept of nanoscale flaw tolerance (Gao et al., 2003; Gao and Ji, 2003) indicated that materials become insensitive to flaws and fail at their theoretical strength as the characteristic size of a structure approaches a critical length in the nanometer regime. This concept has so far been discussed only within the framework of continuum mechanics. Here we conduct atomistic simulations to confirm the flaw tolerance concept from the atomistic point of view.

We focus on a mode I crack in a thin strip of material. If the width of the strip is larger than the critical size for flaw tolerance, failure is governed by the Griffith condition. If the width of the strip is below the critical size for flaw tolerance, failure is no longer governed by the Griffith condition and the solid fails by uniform bond rupture rather than by crack propagation. For the cracked strip of width h subject to an applied strain shown in the inset of Figure 8(a), the energy release rate can be expressed as

$$G = \frac{\sigma^2 h}{2E^*}, \tag{28}$$

where σ is the stress far ahead of the crack tip. Applying the Griffith condition $G = 2\gamma$ yields the critical stress for crack growth

$$\sigma_f = \sqrt{\frac{4\gamma E^*}{h}}. \tag{29}$$

Equation (29) predicts that the critical stress for crack growth increases as the layer width h decreases, approaching infinity as h goes to zero. This is clearly impossible as the stress in the strip can not exceed the theoretical strength σ_{th} of the material. This yields a critical layer width

$$h_{cr} = \frac{4\gamma E^*}{\sigma_{th}^2} \tag{30}$$

below which fracture is no longer governed by the Griffith condition. Note that this expression has the same form as equation (2).

4.1 Atomistic modelling

Atomistic modelling of the strip crack problem is conducted by classical molecular dynamics (MD) simulations using a modified ITAP-IMD code (Stadler et al., 1997; Roth et al., 2000). Consider the geometry depicted in the inset of Figure 8(a). Atoms in the red region are displaced according to a prescribed displacement field. The initial crack extends over half of the slab. The slab size in the x direction is several times larger than that in the y direction. We assume an fcc crystal oriented in cubic orientations, with $x = [100]$, $y = [010]$ and $z = [001]$. The crystal is periodic in the z-direction with crack faces along (010) planes.

We use an energy minimization scheme to relax the crystal after each increment of loading. An increment of strain $\Delta\varepsilon_{yy} = 0.001$ is applied every 3,000 integration steps. Different loading rates are chosen to assure that the results approach equilibrium before the next loading increment is applied. To model a brittle solid, we assume harmonic interactions in the bulk of the strip,

$$\phi(r) = a_0 + \frac{1}{2}k_0(r - r_0)^2, \tag{31}$$

where k_0 is the spring constant, a_0 a reference constant and r_0 the nearest neighbour distance. Crack propagation is constrained along a weak fracture layer in the center of the strip governed by the 12-6 Lennard-Jones (LJ) potential

$$\phi(r) = 4\varepsilon\left(\left(\frac{\sigma}{r}\right)^{12} - \left(\frac{\sigma}{r}\right)^{6}\right). \tag{32}$$

In the simulations, we take $\varepsilon = \sigma = 1$ and $r_0 = 2^{1/6}$. Atoms in the bulk of the strip only interact with their

nearest neighbours, and interactions across the weak fracture layer are cut off at a critical distance $r_{cut} = 2.5$. This setup is chosen because E can be easily varied independent of the other variables in equation (30), allowing h_{cr} to be tuned in a range easily accessible to the MD simulations. The simulation result are expressed in reduced units: energies are scaled by the depth of the LJ potential ε and lengths are scaled by σ.

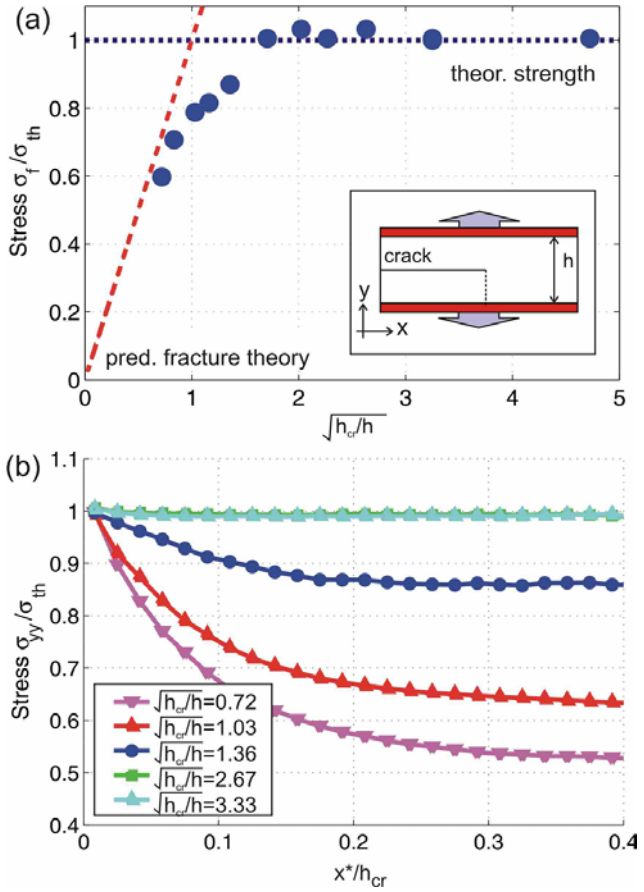

Figure 8 : Atomistic simulations of the flaw tolerance concept. (a) Strength of a cracked nanostrip. The plot shows that the critical stress for failure versus the inverse of the square root of the layer width normalized by the critical length. The failure stress of the cracked nanostrip approaches the theoretical strength as the layer width decreases. (b) Stress distribution ahead of the crack just before failure. The thinner the slab, the more homogeneous is the stress distribution.

For the analysis of the critical length for flaw tolerance, exact knowledge of elastic properties and fracture surface energy is needed. It can be shown that Young's modulus is $E = 4r_0^2 k_0/3$, Poisson's ratio is $\nu = 1/3$; the surface energy is $\gamma = N_b \rho_A \Delta\phi/2$ where N_b is the number of bonds per atom across the fracture path, ρ_A is the density of surface atoms and $\Delta\phi$ is the potential energy stored in each bond. For the (010) fracture surface, $\rho_A = 1/r_0^2 \approx 0.794$, and $N_b = 4$. The potential energy difference per bond is $\Delta\phi \approx 1$. The elastic properties and fracture surface energy are summarized in Table 1.

Table 1 : Elastic properties and surface energy associated with the atomistic model of a cracked nanostrip.

Spring constant k_0	Young's modulus E	Poisson ratio ν	Surface energy γ
572	960	0.33	3.1227

The atomic stress is calculated based on the virial theorem (Tsai, 1979; Marc and McMillan, 1985; Zhou, 2003). Recent investigations have shown that the atomistic definitions of stress near a moving crack tip show reasonable agreement with continuum mechanics predictions (Buehler et al., 2003).

4.2 Simulation results

Figure 8(a) plots the critical failure stress normalized by the theoretical strength, indicating a smooth transition between crack propagation governed by the Griffith condition for thick layers ($\sqrt{h_{cr}/h} < 1$) to uniform rupture at theoretical strength for thin layers ($\sqrt{h_{cr}/h} > 1$). This result is fully consistent with previous analysis based on continuum mechanics (Gao et al., 2003; Gao and Ji, 2003). Figure 8(b) plots the distribution of normal stress ahead of the crack just before failure occurs. As the strip width is decreased, stress concentration at crack tip disappears as the stress distribution becomes more and more uniform near the crack tip. For thicker layers, significant stress magnification develops near the crack and failure occurs by crack propagation.

We have also performed similar calculations when the entire slab is modelled by the LJ potential. Similar transition to flaw tolerant behaviour is observed, with critical length in agreement with the continuum analysis of Gao and Ji (2003).

5 Summary

This paper is aimed to provide a unified treatment of flaw tolerant nanostructures of biological systems. The selection of nanometer scale is shown to be the key for mineral platelets in bone-like biological materials (Gao et al., 2003) to achieve optimum strength in the presence of pre-existing cracks, and for the spatula structure of Gecko to achieve optimum adhesive strength in the presence of adhesion flaws. At a nanometer critical length determined by fracture energy, Young's modulus and theoretical strength, the mineral crystals in biocomposites become insensitive to pre-existing crack-like flaws and the strength of mineral can be maintained near the theoretical strength of the material despite of defects. Following the same principle, the nanometer size of spatula, the most terminal adhesive structure of gecko, achieves maximum adhesion strength and become tolerant of potential contact flaws. We have used simple models to estimate the stiffness and fracture energy of biocomposites. The analysis has helped identify the important parameters responsible for the superior mechanical properties achieved by biological nanostructures. In the protein-mineral nanocomposites, large aspect ratios of mineral platelets are shown to compensate for the low modulus of protein, allowing the biological materials to achieve a high stiffness close to that of mineral. The high fracture energy of biocomposites is the combined property of ultra strong mineral platelets interspersed among protein molecules which undergo extraordinarily large deformation via domain unfolding and interface slipping under a large effective shear stress. Cross-link mechanisms such as Ca^{++} induced sacrificial bonds in bone increase the shear stress in protein and along the protein-mineral interface, effectively converting the behavior of entropic elasticity of biopolymers to one that resembles metal plasticity. Such mechanisms not only build up a large effective stress in protein but also allow protein deformation and interface slipping to occur simultaneously under similar stress levels, making it possible to engineer a very long range of deformation under significant stress in order to maximize energy absorption. Optimization of mineral platelets near theoretical strength allows a large effective stress to be built up in protein via cross-link mechanisms. In this way, the mineral platelets provide the required stiffness for mechanical support of biological systems and protein plays the role of absorbing and dissipating large quantities of fracture energy.

It is interesting to note that the protein-mineral structure of biocomposites is consistent with the ancient Chinese philosophy that combination of "Ying" and "Yang", things of complementary nature or properties, results in perfection and harmony in nature. In biological materials, one may identify many complementary properties such as: (1) stiff versus soft, (2) hard versus gentile, (3) brittle versus ductile, (4) strong versus weak, (5) long versus short, (6) tension versus shear, (7) dissipative versus non-dissipative, etc. In biological materials, the mineral platelets act as the "yang" phase which possesses the "yang" characters like stiff, hard, brittle, non-dissipative, non-yielding, and provides the stiffness of the structure. In contrast, the protein acts as the "ying" phase which possesses the "ying" characters such soft, gentile, ductile, dissipative, flexible and plays the main role of dissipating fracture energy and achieving a high fracture toughness. It is most interesting to note that the nanometer scale plays the key role in the property optimization of mineral-protein structure.

We have used continuum (Gao et al., 2003; Gao and Ji, 2003) and atomistic simulations to investigate the concept of nanoscale flaw tolerance. The atomistic simulations complement continuum analysis and reveal a smooth transition between Griffith mode of failure via crack propagation to uniform bond rupture at theoretical strength below a nanometer critical length, as shown in Figure 8(a). Below the critical length for flaw tolerance, the stress distribution becomes uniform near the crack tip, as shown in Figure 8(b). The atomistic simulations thus fully support the conjecture of Gao et al. (2003) that materials become insensitive to flaws below a critical nanometer length scale.

6 Future perspectives

Understanding engineering principles of biological systems can play an important role in helping address some of the major challenges in materials science and engineering in the 21^{st} century. The development of nanotechnology will eventually open up enormous possibilities in developing multi-functional and hierarchical materials systems. What we have discussed in this paper regarding the bulk and surface nanostructures of biological systems is only a small step in this grand endeavour. In some cases, such as those discussed in this paper, convergent evolutions occur when genetically unrelated biological systems have adopted the same strategies to achieve

the same objectives or properties or functions. In other cases, genes associated with a given set of properties or functions of the same biological system may be found to be strongly conserved over the history of evolution. Whenever convergent evolutions occur, we may look for hints on property optimization. We have discussed in this paper strength, stiffness, toughness and adhesion in connections with the principle of nanoscale flaw tolerance. Similar investigations may be conducted with respect to other properties including friction, fatigue, corrosion and hydrophobicity. There is still a long way to go before the complexities and basic principles of hierarchical structures of biological systems and their associated functions are fully understood.

The investigation reported in this paper underlines the importance of a coherent study of mechanics and chemistry of biological systems. Nature does not distinguish between material and structure. Through the examples of biological nanostructures, we wish to emphasize that mechanics (structure) and chemistry (material) are used with equal importance to achieve optimized materials properties.

Acknowledgement: Support of this work has been provided by the Max Planck Society, the National Science Foundation of China and the Chang Jiang Scholar program through Tsinghua University. MJB acknowledges the Institute for Theoretical and Applied Physics at the University of Stuttgart for providing their MD simulation code.

References

Arzt, E.; Enders, S.; Gorb, S. (2002): Towards a micromechanical understanding of biological surface devices, *Z. Metallk.*, Vol. 93, pp.345-351.

Arzt, E.; Gorb, S.; Spolenak, R. (2003): From micro to nano contacts in biological attachment devices, *Proc. Natl. Acad. Sci. USA*, Vol. 100, pp.10603-10606.

Autumn, K.; Liang, YA.; Hsieh, S. T.; Zesch, W.; Wai, P. C.; Kenny, T. W.; Fearing, R.; Full, R. J. (2000): Adhesive force of a single gecko foot-hair, *Nature*, Vol. 405, pp.681-685.

Autumn, K.; Sitti, M.; Liang, Y. A.; Peattie, A. M.; Hansen, W. R.; Sponberg, S.; Kenny, T. W.; Fearing, R.; Israelachvili, J. N.; Full, R. J. (2002): Evidence for van der Walls adhesion in gecko setae, *Proc. Natl. Acad. Sci. USA*, Vol. 99, pp.12252-12256.

Buehler, M. J.; Gao, H.; Huang, Y. (2003): Atomic and continuum studies of a suddenly stopping supersonic crack, *Comp. Mater. Sci.*, Vol. 28, No. 3-4, pp.385-408.

Buehler, M. J.; Abraham, F. F.; Gao, H. (2003): Hyperelasticity governs dynamic fracture at a critical length scale, *Nature*, Vol. 426, pp.141-146.

Currey, J. D. (1977): Mechanical properties of mother of pearl in tension, *Proc. R. Soc. London B*, Vol. 196, pp.443-463.

Currey, J. D.; Taylor, J. D. (1974): The mechanical behavior of some molluscan hard tissues, *J. Zool.*, Lond., Vol. 173, pp.395-406.

Dugdale, D. S. (1960): Yielding of steel sheets containing slits, *J. Mech. Phys. Solids*, Vol. 8, pp.100-104.

Fratzl, P.; Jakob, H. F.; Rinnerthaler, S.; Roschger, P.; Klaushofer, K. (1997): Position resolved small-angle X-ray scattering of complex biological materials, *J. appl. Cryst.*, Vol. 30, pp.765-769.

Gao, H.; Ji, B. (2003): Modeling fracture in nanomaterials via a virtual internal bond method, *Engng. Frac. Mech.*, Vol. 70, pp.1777-1791.

Gao, H.; Ji, B.; Jaeger, I. L.; Arzt, E.; Fratzl, P. (2003): Materials become insensitive to flaws at nanoscale: lessons from nature, *Proc. Natl. Acad. Sci. USA*, Vol. 100, pp.5597-5600.

Gao, H.; Wang, X.; Yao, H.; Gorb, S.; Arzt, E. (2004): Mechanics of hierarchical adhesion structure of gecko, *Mech. Mat.*, in the press.

Griffith, A. A. (1921): The phenomena of rupture and flow in solids, *Phil. Trans. R. Soc. London A*, Vol. 221, pp.163-198.

Hui, C. Y.; Jagota, A.; Lin, Y. Y.; Kramer, E. J. (2002): Constraints on microcontact printing imposed by stamp deformation, *Langmuir*, Vol. 18, pp.1394-1407.

Jackson, A. P.; Vincent, J. F. V.; Turner, R. M. (1988): The mechanical design of nacre, *Proc. R. Soc. London B*, Vol. 234, pp.415-440.

Jaeger, I.; Fratzl, P. (2000): Mineralized collagen fibrils: A mechanical model with a staggered arrangement of mineral particles, *Biophys. J.*, Vol. 79, pp.1737-1746.

Ji, B.; Gao, H. (2004a): A study of fracture mechanisms in biological nano-composites via the virtual internal bond model, *Mater. Sci. Engng. A*, Vol. 366,

pp.96-103.

Ji, B.; Gao, H. (2004b): Mechanical properties of a generic nanostructure of biomaterials, *J. Mech. Phys. Solids*, in the press.

Johnson, K. L.; Kendall, K.; Roberts, A. D. (1971): Surface energy and the contact of elastic solids, *Proc. R. Soc. London A*, Vol. 324, pp.301 -313.

Kamat, S.; Su, X.; Ballarini, R.; Heuer, A. H. (2000): Structural basis for the fracture toughness of the shell of the conch strombus gigas, *Nature*, Vol. 405, pp.1036-1040.

Klein, P.; Gao, H. (1998): Crack nucleation and growth as strain localization in a virtual-bond continuum, *Engng. Frac. Mech.*, Vol. 61, pp.21-48.

Landis, W. J. (1995): The strength of a calcified tissue depends in part on the molecular structure and organization of its constituent mineral crystals in their organic matrix, *Bone*, Vol. 16, No. 5, pp.533-544.

Landis, W. J.; Hodgens, K. J. (1996): Mineralization of collagen may occur on fibril surfaces. Evidence from conventional and light-voltage electron microscopy and three-dimensional imaging. , *J. Struct. Biol.*, Vol. 117, pp.24-35.

Marc, G.; McMillan, W. G. (1985): The virial theorem, *Adv. Chem. Phys.*, Vol. 58, pp.209-361.

Menig, R.; Meyers, M. H.; Meyers, M. A.; Vecchio, K. S. (2001): Quasi-static and dynamic mechanical response of strombus gigas (conch) shells, *Mater. Sci. Engng. A*, Vol. 297, pp.203-211.

Menig, R.; Meyers, M. H.; Meyers, M. A.; Vecchio, K. S. (2000): Quasi-static and dynamic mechanical response of haliotis rufescens (abalone) shells, *Acta Mater.*, Vol. 48, pp.2383-2398.

Okumura, K.; de Gennes, P. -G. (2001): Why is nacre strong? Elastic theory and fracture mechanics for biocomposites with stratified structures, *Eur. Phys. J.*, Vol. E 4, pp.121-127.

Persson, B. N. J. (2003): On the mechanism of adhesion in biological systems, *J. Chem. Phys.*, Vol. 118, pp.7614-7621.

Rho, J. Y.; Kuhn-Spearing, L.; Zioupos, P. (1998): Mechanical properties and the hierarchical structure of bone, Med. *Engng. Phys.*, Vol. 20, pp.92-102.

Roschger, P.; Grabner, B. M.; Rinnerthaler, S.; Tesch, W.; Kneissel, M.; Berzlanovich, A.; Klaushofer, K.; Fratzl, P. (2001): Structural development of the mineralized tissue in the human L4 vertebral body, *J. Struct. Biol.*, Vol. 136, pp.126-136.

Roth, J.; Gähler, F.; Trebin, H-R. (2000): A molecular dynamics run with 5.180.116.000 particles, *Int. J. Mod. Phys. C*, Vol. 11, pp. 317-322.

Scherge, M.; Gorb, S. N. (2001): Biological Micro and Nano-Tribology, Springer-Verlag, New York.

Smith, B. L.; Schaeffer, T. E.; Viani, M.; Thompson, J. B.; Frederick, N. A.; Kindt, J.; Belcher, A.; Stucky, G. D.; Morse, D. E.; Hansma, P. K. (1999): Molecular mechanistic origin of the toughness of natural adhesive, fibres and composites, *Nature*, Vol. 399, pp.761-763.

Stadler, J.; Mikulla, R.; Trebin, H-R. (1997): IMD: A Software Package for Molecular Dynamics Studies on Parallel Computers, *Int. J. Mod. Phys. C*, Vol. 8, pp.1131-1140

Tada, H.; Paris, P. C.; Irwin, G. R. (2000): The stress analysis of cracks handbook. *ASME Press*, New York.

Taylor, J. D. (1973): The structural evolution of the bivalve shell, *Palaeontology*, Vol.16, pp.519-534.

Tesch, W.; Eidelman, N.; Roschger, P.; Goldenberg, F.; Klaushofer, K.; Fratzl, P. (2001): Graded microstructure and mechanical properties of human crown dentin, *Calcif. Tissue Int.*, Vol. 69, pp.147-157.

Thompson, J. B.; Kindt, J. J.; Drake, B.; Hansma, H. G.; Morse, D. E.; Hansma, P. K. (2001): Bone indentation recovery time correlates with bond reforming time, *Nature*, Vol. 414, pp.773-776

Tsai, D. H. (1979): The virial theorem and stress calculation in molecular dynamics, *J. Chem. Phys.*, Vol. 70, No.3, pp.1375-1382.

Wang, R. Z.; Suo, Z.; Evans, A. G.; Yao, N.; Aksay, I. A. (2001): Deformation mechanisms in nacre, *J. Mater. Res.*, Vol. 16, pp.2485-2493.

Warshawsky, H. (1989): Organization of Crystals in Enamel. Anat. Rec. Vol. 224, pp.242-262.

Weiner, S.; Veis, A.; Beniash, E.; Arad, T.; Dillon, J. W.; Sabsay, B.; Siddiqui, F. (1999): Peritubular dentin formation: crystal organization and the macromolecular constituents in human teeth, *J. Struct. Biol.*, Vol. 126, pp.27-41.

Weiner, S.; Wagner, H. D. (1998): The material bone: Structure-mechanical function relations, *Ann. Rev. Mater. Sci.*, Vol. 28, pp.271-298.

Zhou, M. (2003): A New Look at the Atomic Level Virial Stress – On Continuum-Molecular System Equivalence, *Proc. R. Soc. London A*, Vol. 459, pp.2347-2392.